Int. J. Electrochem. Sci., 17 **(2022)** Article Number: 220556, doi: 10.20964/2022.05.55

International Journal of
ELECTROCHEMICAL
SCIENCE
www.electrochemsci.org

The Synergistic Inhibition Effect between Imidazoline and 2-Mercaptoethanol on Carbon Steel Corrosion in CO_2-saturated 3.5% NaCl solution

Xiaolin Yue[1], *Qiang Wei*[2], *Yuan Lu*[2], *Ming Duan*, *Hu Wang*[1,*], *Juan Xie*[1,*]

[1] School of New Energy and Materials, Southwest Petroleum University, Chengdu 610500, China
[2] CenerTech Oilfield Chemical Co., Ltd., CNOOC, Tianjin, 300450
[3] College of Chemistry and Chemical Engineering, Southwest Petroleum University, Chengdu 610500, China
[*]E-mail: senty78@126.com (Hu Wang), jennyx99@126.com (Juan Xie)

Received: 15 September 2021 / *Accepted:* 13 December 2021 / *Published:* 5 April 2022

The synergistic effect of oleic-based imidazoline (OIM) and mercaptoethanol (ME) on the corrosion of carbon steel in produced water of petroleum exploitation was investigated using weight-loss, electrochemical measurements and X-ray photoelectron spectroscopy (XPS). Results showed that OIM-ME mixtures greatly reduced the corrosion rate of carbon steel, and raised the inhibition efficiency up to 89.6%, compared with individual OIM (73.1%) or ME (56.3%). The OIM-ME mixture is a mixed-type corrosion inhibitor, and the optimal molar ratio is 1:3. Based on EIS spectra and XPS surface analysis, a bilayer adsorption model was proposed to illustrate the synergistic inhibition mechanism.

Keywords: CO_2 Corrosion; Inhibitor; Synergistic Inhibition Effect; Imidazoline; Mercaptoethanol

1. INTRODUCTION

Carbon dioxide (CO_2) is usually found in amounts of different levels in oil and gas exploitation. And CO_2 could be very corrosive to metallic equipment served in oilfield system, when it is dissolved into produced liquid, often mixture of brine water and crude oil [1-6]. The dissolution of CO_2 into produced liquid can lead to the decrease of pH value, bringing about severe acidic corrosion. This kind of corrosion is usually known as “sweet corrosion”, which is a major problem in the oil and gas industry, causing great economic losses and threatening the safety of oil and gas exploitation equipment and transportation pipelines [7-9].

Carbon steels are widely used in oil and gas industry for their relatively low cost, good machining performance and acceptable corrosion resistance. However, carbon steel equipment, casing pipeline for

instance, is quite sensitive to "sweet corrosion" environment and easily corrode. In another hand, CO_2 corrosion is a complex procedure which could be affected by many factors, such as temperature, partial pressure of acidic gas, water content, solid particles, flow rate of fluids, salinity, presence and concentration of hydrogen sulfide, materials condition, and so on [10-13]. Therefore, it is still of great significance to pay more attention to the investigation of CO_2 corrosion. And it is also urgent that better corrosion control methods must be found to prevent or alleviate CO_2 corrosion of carbon steels.

Among numerous corrosion protection methods, corrosion inhibitor is widely used and acts as one of the most economical and effective ways to defend corrosion attack in industrial area, especially in oil and natural gas exploitation system [7-8, 14-15]. Organic inhibitors, which contain groups of nitrogen, oxygen, sulfur and phosphorus, have been proved to be quite effective both in laboratory and in practical applications [16-20]. Imidazoline and its derivatives have been used extensively as corrosion inhibitors in present petroleum industry, not only in exploitation, but also in oilfield ground system, transportation system and refinery for their good anticorrosion effect. In order to obtain better corrosion inhibition performance and reduce the applied dosage, mixtures of various chemicals with imidazoline are commonly used in practice, which can produce a synergistic effect. The synergistic effect between these chemicals ensures a better anticorrosion performance, lower cost and more convenience for practical operation. Recent years, researchers have been dedicated to the discovery of new synergistic inhibitors as well as the investigation of their synergism, for the limited corrosion inhibition performance of individual application of imidazoline.

The synergistic inhibition effect between imidazoline and other chemicals, such as thiourea, halides and benzoate salts etc., has been reported [1, 14, 21-23]. J. M. Zhao et al. [22] studied the synergistic inhibition effect of imidazoline and sodium benzoate on the corrosion of carbon steel in CO_2-satuated brine solution. The authors found that there was obvious synergistic effect between imidazoline and sodium benzoate as sodium benzoate could strengthen the inhibition of imidazoline. An adsorption model was also mentioned to illustrate the synergistic adsorption mechanism. J. Z. Ai et al. [24] reported synergism of imidazoline and potassium iodide (KI) for inhibiting galvanic corrosion. The study demonstrated that I^- could change the distribution of excess charge on galvanic electrode, which enhanced the adsorption of imidazoline on both electrodes. P. C. Okafor et al. [1] also found synergism between quaternary imidazoline and iodide ions on mild steel in acidic solution. The corrosion inhibition effect is due to physical adsorption of quaternary imidazoline on the surface of mild steel, and a mixed-inhibition mechanism is proposed. The synergism of imidazoline and thiourea had also been investigated [25]. The results suggested that the presence of imidazoline stabilized the adsorption of thiourea molecules on the interface and the adsorption process was regarded as Langmuir adsorption. However, the synergistic inhibition mechanism reported was mainly focused on the base of a relatively low temperature (30 ℃ or lower) which differs far from lots of industrial applications.

Although inhibition mechanism of imidazolines and its derivatives have been extensively studied in acidic solution, investigation on synergistic effect of imidazoline with other chemicals is still relatively scarce and far from well understood. It is significant to improve the corrosion resistance of carbon steel and uncover the synergistic inhibition mechanism under "sweet corrosion" environment. Meanwhile, the comprehension of synergistic inhibition mechanism is quite helpful to design, synthesize and develop a series of new inhibitors which are much more efficient, economical and environment-friendly. In this

paper, the synergism of oleic-based imidazoline (OIM) and mercaptoethanol (ME) on the corrosion of carbon steel in CO_2-saturated 3.5% NaCl solution at 65℃ was studied by weight-loss method and electrochemical measurements. In addition, surface analysis by XPS has also been performed to characterize the film formed at the electrode/solution interface. Furthermore, a bilayer adsorption model has been proposed to illustrate the synergistic inhibition mechanism.

2. EXPERIMENTAL

2.1. Experimental samples

The test material was mild steel Q235 with the chemical composition (wt%) of C 0.16, Mn 0.53, Si 0.30, S 0.045, P 0.015 and Fe (bal). All samples were ground to P2000 grit SiC paper, rinsed in an ultrasonic bath with acetone, and dried in cold air before experiments.

2.2. Experimental solution

3.5% NaCl solution was used as the blank solution. The pH value of the solution, saturated with CO_2 gas, was 4.3 (65℃).

The structures of OIM (Shengli Co. Ltd., China) and ME (Kelong Co. Ltd., China) are shown in Fig. 1. The purity of OIM is approximately 96%. ME was analytical grade. The inhibitor concentration of OIM and ME was 2×10^{-4} mol·L^{-1}. The experiment temperature was 65℃.

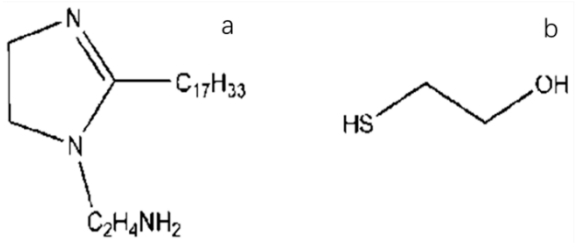

Figure 1. Structure of oleic-based imidazoline and mercaptoethanol: a. OIM; b. ME.

2.3. Weight-loss measurements

In the weight-loss measurements, samples with the size of 40 mm×13 mm×2 mm were immersed in flasks with a total volume of 500 ml 3.5% NaCl solution. Prior to the test, CO_2 was introduced into the solution for 1 hour (h) to remove oxygen. After immersion for 72 h, samples were taken out of the corrosive electrolyte and the surface corrosion products were removed by chemical descaling solution (10% HCl + 0.5% hexamethylenetetramine, $C_6H_{12}N_4$) in ultrasonic cleaner for 5 min. All samples were weighed by an analytical balance (with a precision of 0.1 mg) before and after the tests. Tests were conducted three times for each condition.

2.4. Electrochemical experiments

The electrochemical experiments were performed by a potentiostat (Holland IviumStat). The measurements were carried out in a conventional three electrodes cell which is composed of working electrode (WE), saturated calomel reference electrode (SCE) with a Luggin capillary salt bridge and a platinum counter electrode (CE). The WE surface area exposed to the aggressive solution was 1 cm^2. The test temperature was 65±1℃. Saturated CO_2 condition was obtained by passing CO_2 gas into the 3.5% NaCl solution for 1 h before tests and all through the electrochemical experiments.

The potentiodynamic polarization measurements were conducted after 2 h in-situ monitoring of OCP in both inhibited and uninhibited solution. The potential was scanned from -500 to +700 mV (vs. OCP), with scan rate of 0.5 $mV \cdot s^{-1}$.

The EIS measurements were conducted at E_{ocp} with a perturbation amplitude of 5 mV and a frequency range from 100 kHz to 1 mHz. Before the tests, 2 h in-situ monitoring of OCP was performed to ensure a relatively stable state of the electrode surface. Equivalent circuit software, ZSimpWin3.10, was used to fit the EIS spectrum.

2.5. X-ray photoelectron spectroscopy test

The XPS spectra were performed on samples surface after immersed for 4 h. Spectrometer AXIS Ultra DLD (KRATOS ANALYTICAL, UK) with an ultra-high vacuum chamber (pressure below 1.0×10^{-8} Pa, Mg K_α radiation) was used. Binding energies are referenced to C (1s) fixed at 284.6 eV [26].

3. RESULTS AND DISCUSSION

3.1. Weight-loss measurement

The corrosion rates (CRs) of the carbon steel was calculated using the following equation:

$$\mathrm{CR} = \frac{\Delta \mathrm{m}}{\mathrm{St}} \quad (1)$$

Where Δm is the average weight loss of three identical samples, S is the exposed surface area of the sample and t is immersion time.

And the inhibition efficiencies (IE%) of the corrosion inhibitors were calculated by the corrosion rates (CRs):

$$\mathrm{IE\%} = \left(1 - \frac{\mathrm{CR}}{\mathrm{CR}'}\right) \times 100 \quad (2)$$

Where CR and CR′ is the corrosion rate of carbon steel with and without inhibitors in aggressive solution, respectively.

Table 1 presents the values of corrosion rates (CRs) of carbon steel in the absence and presence of corrosion inhibitors in CO_2-saturated 3.5% NaCl solution at 65℃, and the inhibition efficiencies (IE%) of corrosion inhibitors.

It is observed that the corrosion rate is very high in the absence of corrosion inhibitor. The carbon steel was seriously corroded. The addition of OIM or ME at the concentration of 2×10^{-4} mol·L^{-1} apparently alleviated the severity, indicating a protecting effect against CO_2 corrosion. The inhibition efficiency (IE%) is 73.1% and 56.3% for OIM and ME, respectively. Furthermore, the IE% values exceed 80% when OIM-ME mixtures are added with a total concentration of 2×10^{-4} mol·L^{-1}, which reveals the apparent synergistic inhibition effect of OIM and ME. In addition, the maximum corrosion inhibition efficiency can rise up to 89.6% when the mole ratio of OIM:ME equals to 1:3.

Table 1. CR and IE% values of mild steel with and without inhibitors (2×10^{-4} mol·L^{-1}) in CO_2-saturated solution by weight-loss measurement.

Inhibitor addition	CR/g m^{-2} h^{-1}	IE%
Blank	0.5773	-
OIM	0.1553	73.10
ME	0.2523	56.30
OIM:ME=5:1	0.0961	83.34
OIM:ME=3:1	0.0835	85.55
OIM:ME=1:1	0.0763	86.80
OIM:ME=1:3	0.0600	89.61
OIM:ME=1:5	0.1002	82.65

3.2. Potentiodynamic polarization experiment

Before the potentiodynamic polarization measurement, OCP was monitored for 2 h. The OCP variations with time were presented in Fig. 2a. It can be seen that OCP value keeps at about -0.73 V in the absence of corrosion inhibitor. In the presence of inhibitor, the corrosion potential is higher in comparison. It indicates that the presence of corrosion inhibitor makes the metal surface more stable thermodynamically. It is also worth noticing that OCP values fluctuate significantly in the presence of inhibitor, especially in the presence of OIM. The fluctuations reveal the dynamic adsorption and equilibrium of corrosion inhibitors at the electrode/solution interface.

PC measurements confirm the result, as shown in Fig. 2b. With the addition of corrosion inhibitor, the corrosion potential (E_{corr}) becomes much nobler. Both the anodic and cathodic current densities decrease which suggests the anodic dissolution process and the cathodic hydrogen evolution process have been retarded. And the changes of both anodic Tafel slope and cathodic Tafel slope are due to the adsorption of corrosion inhibitors [27]. Furthermore, the addition of OIM-ME mixture can produce a stronger inhibition effect on both anodic dissolution and cathodic hydrogen evolution process than individual addition of OIM or ME. An abrupt increase of corrosion current can be detected on the anodic curve in the presence of OIM-ME mixture when the polarization potential reaches a relatively higher value (around -0.5 V). According to [2, 10, 28], this involves an anodic desorption process of corrosion inhibitors or the attack of Cl^{-1} on the protective film formed by inhibitors.

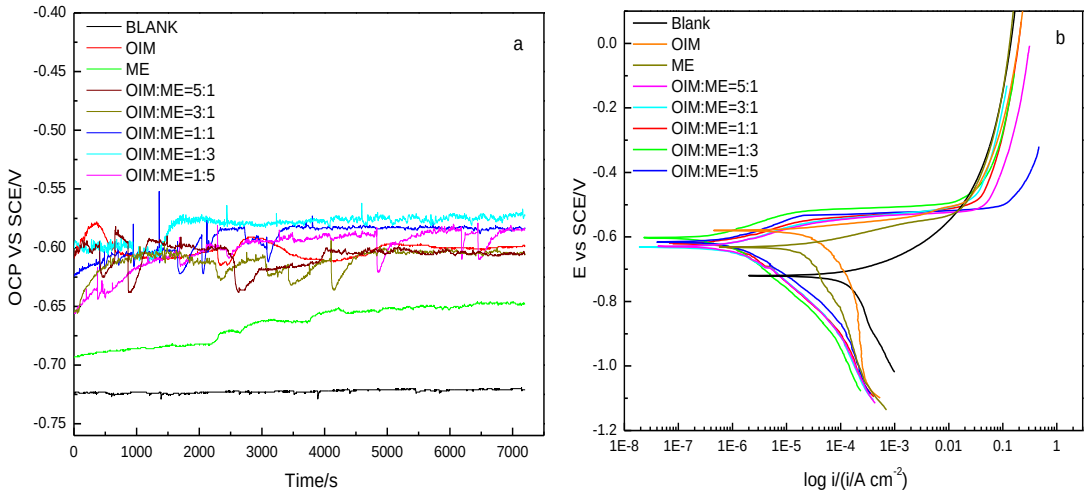

Figure 2. OCP and PC in a CO_2-saturated 3.5% NaCl solution containing 2×10^{-4} mol·L^{-1} corrosion inhibitor and without corrosion inhibitor were obtained at 65℃: a. OCP measurements; b. PC measurements.

Table 2. Electrochemical parameters and inhibition efficiency obtained from polarization curves for mild steel in the CO_2-saturated solution in the absence and presence of different kinds of inhibitors at 65℃.

Fomula	β_a/mV	β_c/mV	E_{corr}/mV	I_{corr}/μAcm^{-2}	IE%
Blank	242	205	-720	92.32	-
OIM	210	290	-581	19.82	78.53
ME	253	238	-634	35.34	61.72
5:1	205	208	-606	2.78	96.98
3:1	230	209	-623	2.31	97.47
1:1	221	206	-618	1.91	97.94
1:3	227	210	-600	1.12	98.78
1:5	179	224	-615	2.92	96.83

Table 3. Comparison of the electrochemical parameters and corrosion inhibition efficiency of several imidazoline corrosion inhibitors in the polarization curve test.

Inhibitors	concentration	conditions	Polarization method			Reference
			E_{corr}(V)	I_{corr}(mA/cm^2)	η%	
2UMQI+KI	1.4×10^{-4} mol·L^{-1} 2UMQI +0.1mol·L^{-1} KI	25℃, 1.0 M H_2SO_4 solution	-0.41	0.0595	97.50	[1]
imidazoline phosphate	3.5×10^{-4} mol·L^{-1}	25℃, 1 M HCl solution	-0.63	0.0062	91.45	[21]
CQI	6.2×10^{-4} mol·L^{-1}	25℃, 3% NaCl and 3% Na_2SO_4 CO_2-saturated solution	-0.64	0.0018	98.10	[23]

imidazoline derivative	7.7×10^{-5} mol·L^{-1}	55°C, CO_2-saturated brine solution	-0.67	0.0043	95.30	[38]
imidazoline derivative	1.5×10^{-4} mol·L^{-1}	20°C, 2% NaCl CO_2-saturated solution	-0.62	0.0039	92.70	[39]
TAI	0.9×10^{-4} mol·L^{-1}	25°C, CO_2-saturated brine solution 168h	/	/	96.20	[40]
QIM+ME	2×10^{-4} mol·L^{-1} OIM:ME=1:3	65°C, CO_2-saturated brine solution	-0.60	0.0011	98.78	This work

By Tafel extrapolation method, anodic and cathodic Tafel slopes (β_a, β_c), corrosion potential (E_{corr}) and corrosion current densities (I_{corr}) are calculated, as listed in Table 3. The values of inhibition efficiency IE% are calculated by corrosion current densities (I_{corr}) from the following equation:

$$IE\% = \frac{I'_{corr} - I_{corr}}{I'_{corr}} \times 100 \quad (3)$$

Where I'_{corr} and I_{corr} are the corrosion current densities without and with the addition of corrosion inhibitors, respectively. Inhibition efficiencies (IE%) by I_{corr} are also listed in Table 2.

It is observed from Table 2 that in presence of corrosion inhibitors, E_{corr} remarkably increases. And higher values of E_{corr} are obtained when OIM-ME mixture is added. Besides, both the values of anodic Tafel slope and cathodic slope have changed greatly in presence of OIM-ME mixture, confirming a mixed type of corrosion inhibitor. In addition, the corrosion current density (I_{corr}) sharply decreases with addition of corrosion inhibitors. Consequently, the inhibition efficiency (IE%) increases in presence of OIM-ME mixtures. For example, IE% of OIM-ME mixture (OIM:ME=1:3) is 98.8% in comparison with 78.5% of OIM and 61.7% of ME. Obviously, there is synergistic inhibition effect between OIM and ME. These results are in good agreement with the weight-loss experiment, although there is some deviation of the IE%, due to different methods.

It is noticed both in the case of weight-loss experiment and potentiodynamic polarization measurement that higher inhibition efficiencies are obtained when smaller amounts of OIM (or larger amounts of ME) in the OIM/ME mixture are applied. And when OIM:ME=1:3, the highest inhibition efficiency is obtained. At the same time, it can be seen from Table 3 that compared with the polarization curve test results of imidazoline corrosion inhibitors in other documents, the mixed corrosion inhibitor of OIM:ME=1:3 has higher corrosion inhibition performance. The corrosion inhibition effect may be related to the geometric distribution of OIM and ME molecules at the solution/metal interface. The maximum synergistic inhibition effect can be obtained when the most proper inhibitive film barrier of OIM and ME is formed.

3.3. Electrochemical impedance spectroscopy measurements

The Nyquist and Bode plots of carbon steel in absence and presence of corrosion inhibitors in CO_2-saturated 3.5% NaCl solution at 65°C are shown in Fig. 3. It is observed that introducing individual OIM or ME increases the diameter of the depressed capacitive loop, indicating an inhibition effect of the corrosion process. These depressed semicircles with centers below the real axis are typical characteristics of inhomogeneity of the solid electrode surface and can be ascribed to the frequency dispersion effect [29, 30].

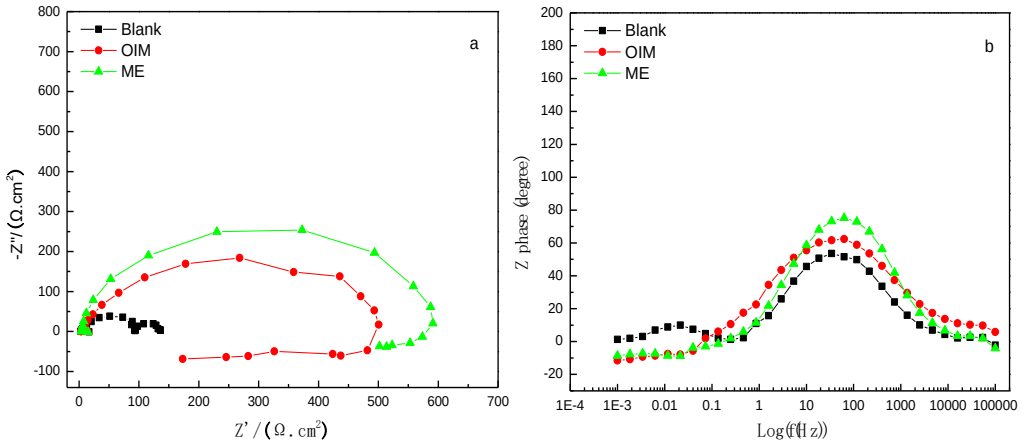

Figure 3. Nyquist and Bode diagrams of carbon steel soaked for 2 h in CO_2-saturated 3.5% NaCl solution at 65°C without or with corrosion inhibitors: a. Nyquist plots; b. Bode plots.

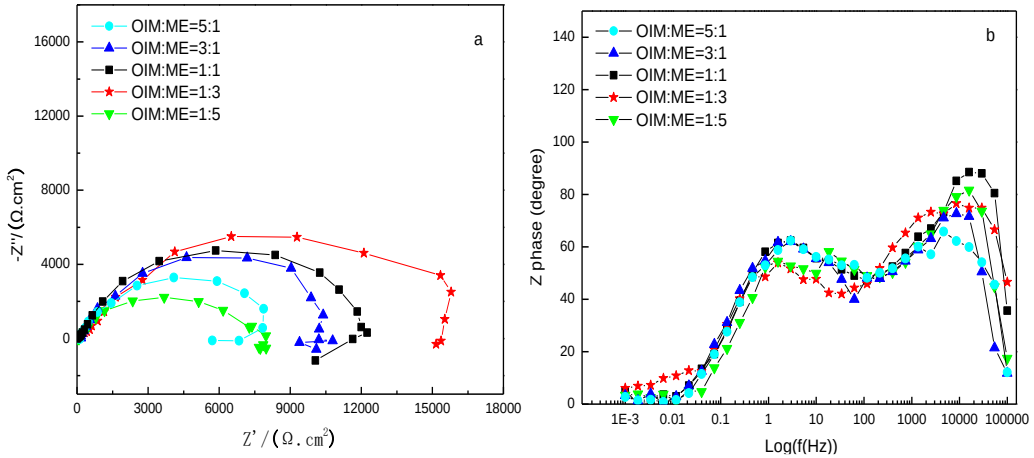

Figure 4. EIS plots of mild steel in CO_2-saturated brine solution with mixed inhibitors of different molar ratios at 65°C after 2h immersion: a. Nyquist plots; b. Bode plots.

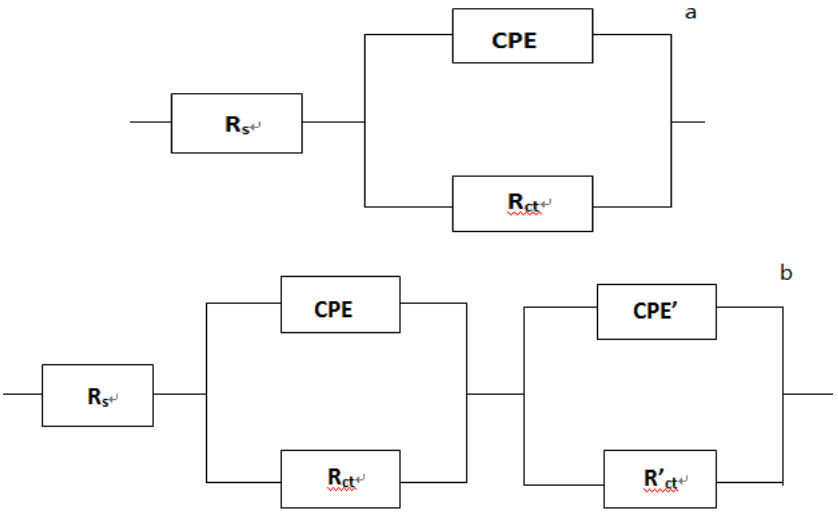

Figure 5. The equivalent circuit used to fit the EIS plots of mild steel in CO_2-saturated brine solution with mixed inhibitors of different molar ratios at 65℃ after 2h immersion: a. the equivalent circuit for OIM or ME; b. the equivalent circuit for the mixture of OIM and ME.

Table 4. Electrochemical impedance parameters obtained from equivalent circuit for mild steel after 2 h immersion in the CO_2-saturated solution in the presence of different kinds of inhibitors at 65℃.

Fomula	R_{ct}/KΩ·cm^{-2}	R_{ct}'/KΩ·cm^{-2}	C/μF·cm^{-2}	C'/μF·cm^{-2}
OIM	0.45	-	283.30	-
ME	0.55	-	77.47	-
5:1	7.28	0.11	80.89	60.80
3:1	8.09	0.12	89.50	41.54
1:1	12.76	0.16	63.20	41.80
1:3	16.12	0.46	59.36	15.58
1:5	7.87	0.11	115.00	53.81

Table 5. Comparison of the electrochemical parameters and corrosion inhibition efficiency of several imidazoline corrosion inhibitors obtained in the EIS test.

Inhibitors	concentration	conditions	EIS method			Reference
			R_{ct} (Ω·cm^2)	C (μF·cm^{-2})	η%	
2UMQI+KI	1.4×10^{-4} mol·L^{-1} 2UMQI +0.1mol·L^{-1} KI	25℃, 1.0 M H_2SO_4 solution	348	26.00	98.56	[1]
imidazoline phosphate	3.5×10^{-4} mol·L^{-1}	25℃, 1 M HCl solution	2300	4.10	92.30	[21]

CQI	6.2×10^{-4} mol·L^{-1}	25℃, 3% NaCl and 3% Na_2SO_4 CO_2-saturated solution	5380	60.00	96.90	[23]
imidazoline derivative	7.7×10^{-5} mol·L^{-1}	55℃, CO_2-saturated brine solution	9320	33.50	91.00	[38]
imidazoline derivative	1.5×10^{-4} mol·L^{-1}	20℃, 2% NaCl CO_2-saturated solution	5010	33.90	92.70	[39]
TAI	0.9×10^{-4} mol·L^{-1}	25℃, CO_2-saturated brine solution 168h	7180	95.30	88.40	[40]
QIM+ME	2×10^{-4} mol·L^{-1} OIM:ME=1:3	65℃, CO_2-saturated brine solution	16120	59.36	98.78	This work

To compare the adsorption dynamic characteristics of OIM-ME mixture with that of OIM and ME, the Nyquist and Bode plots of carbon steel with the addition of OIM-ME mixtures are shown in Fig. 4. The capacitive loop remarkably enlarges when the OIM-ME mixtures are introduced (Fig. 4a). And it is obvious that the ratio of 1:3 (OIM:ME) shows the largest value of capacitive loop, suggesting the optimum ratio among all ratios investigated. This is in good agreement with the result of the weight-loss experiment.

It is notable that the Bode plots of carbon steel in Fig. 3b and Fig. 4b are quite different. One time constant is observed on the Phase angle-Frequency curve of carbon steel in the solution without inhibitor and the solution with individual addition of OIM or ME (as shown in Fig. 3b). However, when OIM-ME mixtures are added, the Phase angle-Frequency curve exhibits two time constants. Therefore, it is believed that two kinds of distribution models of OIM and ME molecules at the electrode/solution interface are possible. One possibility is that OIM and ME molecules distribute alternatively on the same plane. Another one is that they adsorb on different plane and form a bilayer model. In the alternative distribution model, OIM molecules may first block the carbon steel surface, then ME molecules fill in the opening of OIM arrays, suppressing corrosion current dramatically. While in the possible bilayer model, OIM/ME form the first layer then ME/OIM form the second layer. In Fig. 4b, the first time constant emerges at high frequency around 4000 Hz, which usually indicates the presence of a protective inhibitor film over the carbon steel surface. The second time constant emerges in the range from 5 Hz to 20 Hz, which usually characterizes a double layer capacitance, and can be attributed to the formation of a protective film by the adsorption of corrosion inhibitors on the carbon steel surface [31-33]. Therefore, the bilayer adsorption model is much more possible.

The equivalent circuits for fitting the EIS spectra are shown in Fig. 5. The equivalent circuit in Fig. 5a can well fit the spectra of carbon steel in the blank and in the solution with individual addition of OIM or ME. Fig. 5b is the best model for spectra of carbon steel in the solution with OIM-ME mixture among many typical models that have been tried, and accords with bilayer adsorption assumption as well. Parameters such as solution resistance (R_s), charge transfer resistance of the outer and inner interface (R'_{ct}, R_{ct}) and constant phase element (CPE′, CPE) are obtained to illustrate the impedance behavior. Constant phase element (CPE) has been applied to substitute the pure capacitance of the outer and inner interface (C′, C), which accounts for deviations from ideal dielectric behavior related to interface roughness and inhomogeneity [33]. And the impedance of CPE is usually defined as follows:

$$Z_{CPE} = -\frac{1}{Y_0}(2\pi f_{max})^{-n}, 0 < n < 1 \quad (4)$$

Where Y_0 and n are the constant and index of the CPE, respectively. f_{max} is the frequency where the maximum imaginary value ($-Z_{imag}$) emerged. And interface capacitance (C) is usually obtained using the following equation:

$$C = (2\pi f_{max} R_{ct})^{-1} \quad (5)$$

R_{ct} values, corresponding to $-Z_{imag}$, were obtained by fitting the impedance data of Fig. 3 and Fig. 4.

Electrochemical parameters with a fitting error less than 5% are all summarized in Table 4. In presence of inhibitors, the value of charge transfer resistance (R_{ct}) is larger than that of the blank. The increasing R_{ct} values can be explained in the way that the charge transfer process is inhibited. Moreover, in the cases of introducing OIM-ME mixtures, the increase of R_{ct} is much greater compared to the separate addition of OIM or ME. This evidence corresponds to the result of the weight-loss and PC measurements and further confirms the synergistic inhibition effect of OIM and ME. And comparing the AC impedance test results of several imidazoline corrosion inhibitors summarized in Table 5, it can be concluded that adding OIM:ME=1:3 mixed corrosion inhibitor can obtain a larger Rct value and higher corrosion inhibition efficiency. With respect to the decrease in the values of outer interface capacitance (C′) and inner interface capacitance (C), Helmholtz model could be taken into consideration [22]:

$$C = \frac{\varepsilon\varepsilon_0 S}{d} \quad (6)$$

Where ε_0 and ε are the vacuum permittivity constant and dielectric constant of the medium, respectively. S is the electrode area and d is the thickness of the interface layer.

The decrease in the value of the interface capacitance (C) can be attributed to the decline of the dielectric constant ε or the increase in the thickness of the protective layer. It is known that water molecules have large dielectric constant value. The inhibitor molecules with smaller dielectric constant value tend to be preferentially adsorbed onto the substrate and replace water molecules.

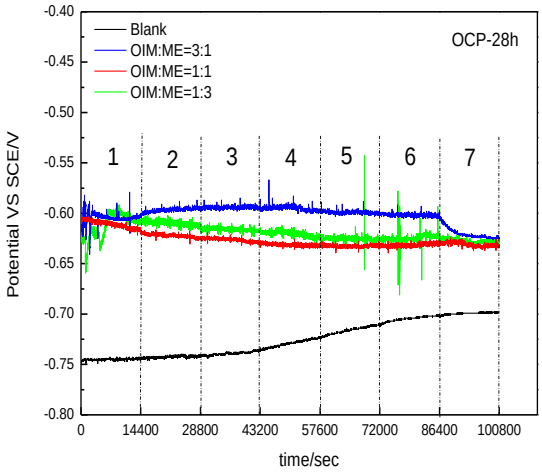

Figure 6. In situ monitoring of the OCP of mild steel in CO_2-saturated brine solution with and without mixed inhibitors during a continuous 28 h measurement at 65℃

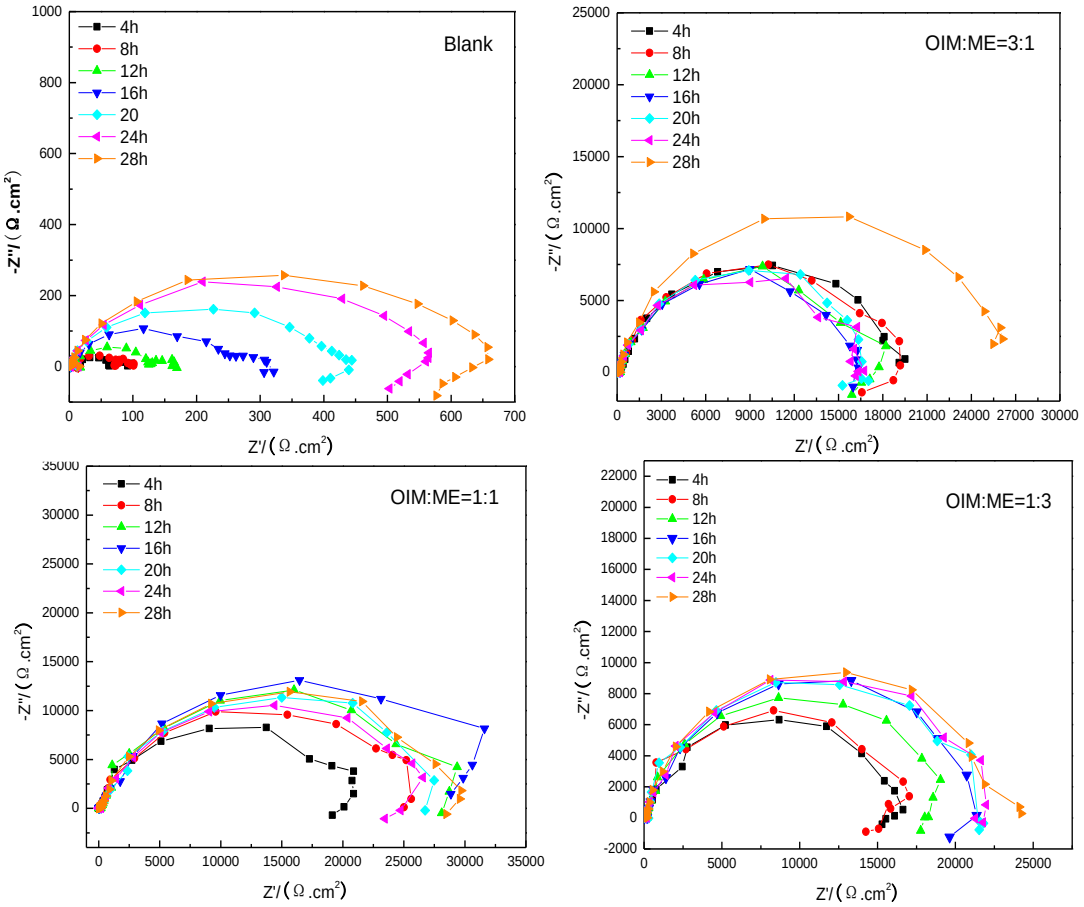

Figure 7. EIS plots of mild steel in CO_2-saturated brine solution with mixed inhibitors in different immersion time at 65℃.

Impedance tests of carbon steel in absence and presence of OIM-ME mixture were also carried out at different immersion time. Prior to each EIS test, 4 h in-situ monitoring of OCP has been recorded

and 28 h of OCP was recorded in total, as shown in Fig. 6. It is observed that the OCP value in the blank solution increases slowly from about -0.75 V to -0.70 V with immersion time, which indicates the formation of a relatively steady corrosion product layer. While in presence OIM-ME mixtures, the OCPs are more positive and apparent fluctuation can be detected. As mentioned above, the fluctuations indicate the dynamic adsorption and equilibrium of corrosion inhibitors at the interface.

To study the change of the adsorption dynamic behavior of OIM-ME mixtures, EIS spectra of carbon steel were recorded each 4 h within 28 h immersion time. Nyquist plots are presented in Fig. 7, of which Fig. 7a is according to the carbon steel in CO_2-saturated 3.5% NaCl solution without inhibitor, Fig. 7b, Fig 7c and Fig. 7d is respectively according to the presence of OIM-ME mixture with the ratio of 3:1, 1:1 and 1:3 (OIM:ME).

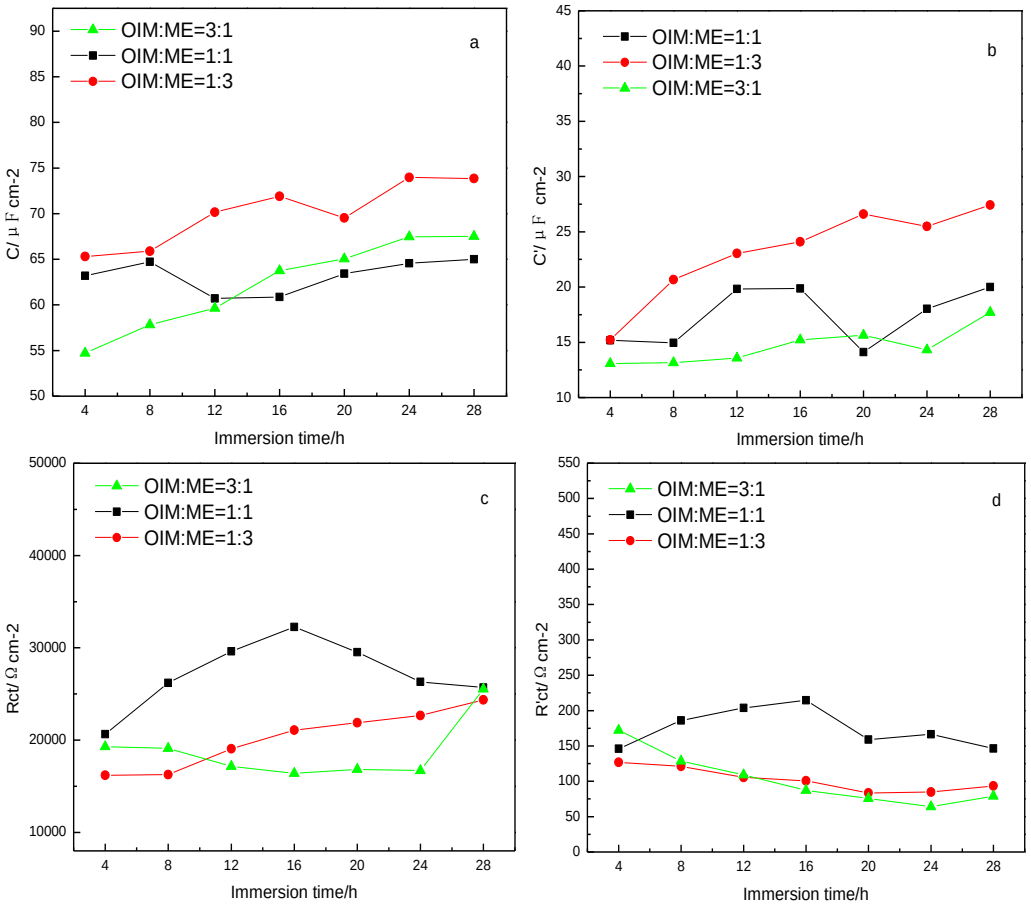

Figure 8. Dependence of R_{ct} and C of mild steel in CO_2-saturated solution with inhibitors on immersion time at 65°C: a. the first interface capacitance; b. the second interface capacitance; the charge transfer resistance of the first interface; d. the charge transfer resistance of the second interface.

Fig. 7a shows that the diameter of the capacitive loop in the Nyquist plots of carbon steel in blank solution increases with immersion time, which can be ascribed to the protective layer formed by corrosion products. It can be observed, from Fig. 7b to Fig. 7d, that in presence of OIM-ME mixtures of different ratios, the capacitive loops are greatly enlarged with immersion time, indicating the effective adsorption of corrosion inhibitors at the electrode/solution interface.

Fig. 8 presents the behavior of charge transfer resistance of carbon steel with OIM-ME mixtures within 28 h immersion time. All values were obtained by fitting the EIS spectra (Fig. 7) with equivalent circuit in Fig. 5b.

It is clear that there is a general increase in the value of outer R_{ct} with immersion time, which characterizes a charge transfer control process (Fig. 8a). And with the ratio of 3:1 and 1:1, minimum and maximum values of R_{ct} were obtained at immersion time of 24 h and 16 h, respectively. While with the ratio of 1:3, R_{ct} keeps increasing within 28 h immersion time, demonstrating a good time-stable ability. As for the inner R'_{ct}, though some fluctuation happened, no significant changes had been observed (Fig. 8b).

According to the results discussed above, it is quite interesting that the corrosion inhibition effect is dependent on the molar ratio of the OIM-ME mixture. This may be resulted from the difference of adsorption kinetic behavior between OIM and ME on the metal/solution surface.

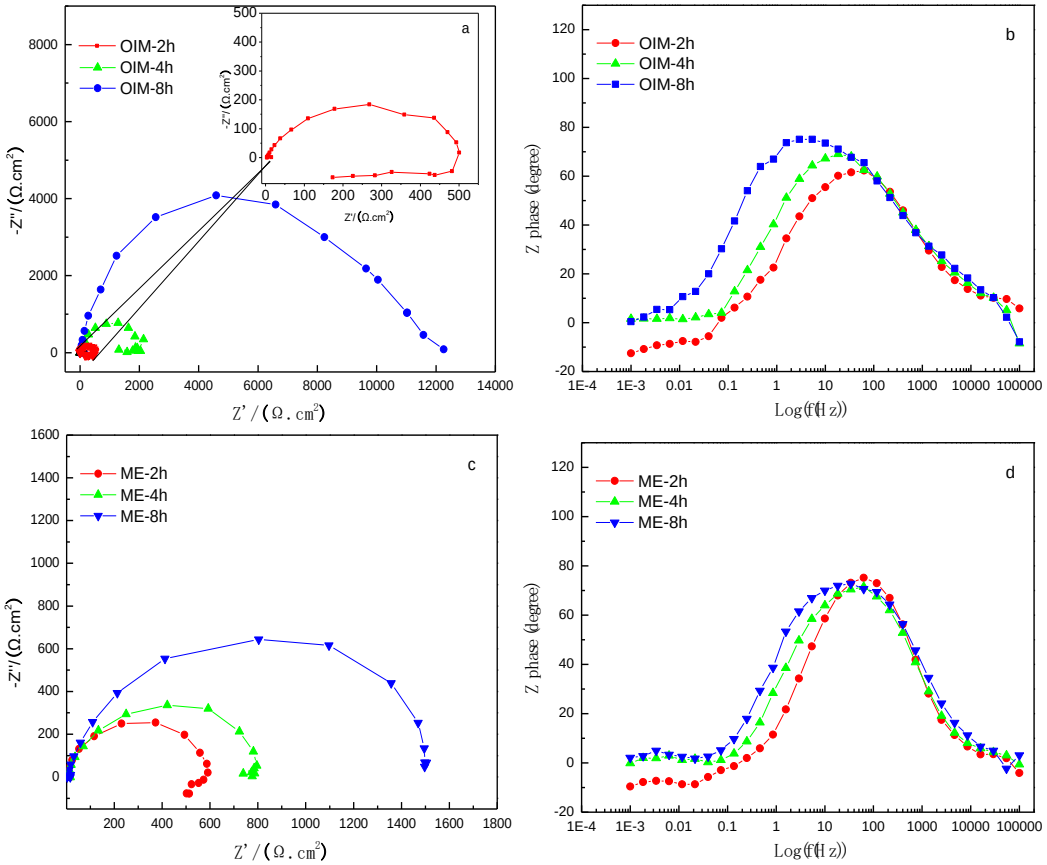

Figure 9. EIS plots of mild steel in CO_2-saturated brine solution with OIM or ME in different immersion time at 65℃: a, b is the Nyquist and Bode plot of OIM respectively; c, d is the Nyquist and Bode plot of ME respectively.

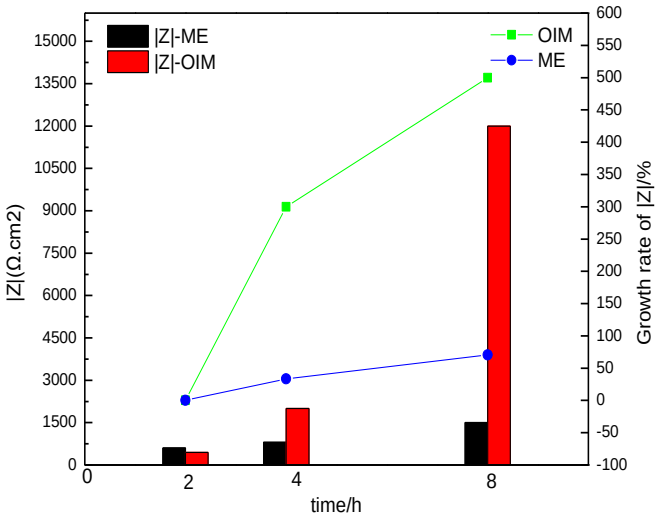

Figure 10. A comparison of the resistance and its growth rate between OIM and ME in different immersion time at 65℃.

Nyquist plots of carbon steel in CO_2-saturated 3.5% NaCl solution with OIM or ME in different immersion time are presented in Fig. 9a and Fig. 9b. A comparison in the increase of the impedance modulus values of carbon steel in the solution with OIM and ME within 8 h is presented in Fig. 9c.

It is observed from Fig. 10 that the impedance modulus value of OIM (about 600 $\Omega \cdot cm^2$) is larger than that of ME (about 400 $\Omega \cdot cm^2$) in the first 2 h immersion. And the impedance modulus of OIM increases faster and is much larger than that of ME when the immersion time exceeds 2 h. Besides, concerning the fact that ME is capable of a smaller molecular structure and greater polarity than OIM, it is possible for ME molecules to be adsorbed onto the surface with priority when the OIM-ME mixture is added. Moreover, evidence from EIS results in Table 3 shows that the charge transfer resistance value of the outer film (R_{ct}) is much larger than that of the inner film (R'_{ct}). Therefore, it can be inferred that a bilayer adsorption film may have been formed on the metal/solution interface, where OIM molecules form the outer film and ME molecules form the inner film. This complex bilayer adsorption film ensures the excellent corrosion resistance of carbon steel in corrosive solution with different immersion time.

3.4. X-ray photoelectron spectroscopy analysis

XPS spectra of carbon steel with corrosion inhibitor film have also been recorded to obtain more detailed information about the adsorption behavior. Samples covered with inhibitor films were obtained by immersing carbon steel into CO_2-saturated 3.5% NaCl solution in the presence of OIM-ME mixtures at 65℃ for 4 h. Carbon steel covered by OIM-ME mixtures of different ratios show similar wide-scan XPS spectra. Therefore, here we just exhibit the wide-scan XPS spectrum of the film formed in the system of 1:3, as presented in Fig. 11.

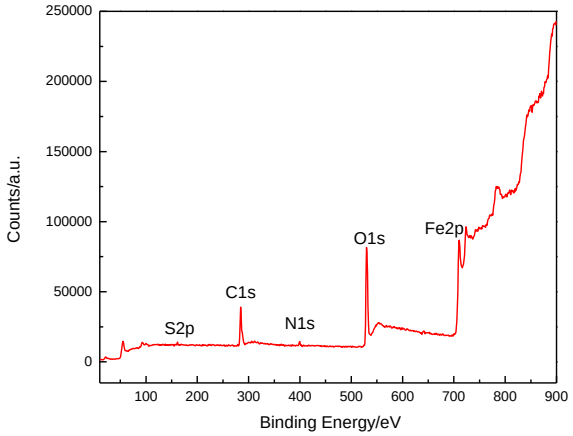

Figure 11. Wide-scan XPS spectra of mild steel obtained after immersion in CO_2-saturated solution at 2×10^{-4} mol·L^{-1} OIM-ME combination with a 4 hours immersion time at 65℃.

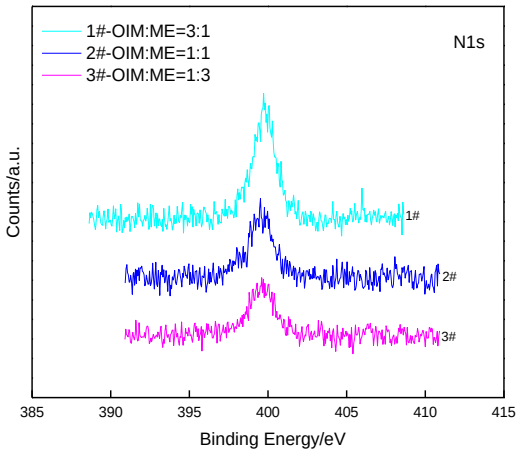

Figure 12. High-resolution XPS spectra of N1s of mild steel obtained after immersion in CO_2-saturated solution at 2×10^{-4} mol·L^{-1} OIM-ME combination with a 4 hours immersion time at 65℃.

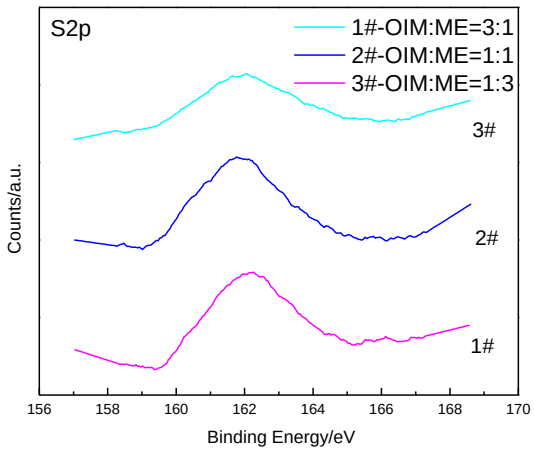

Figure 13. High-resolution XPS spectra of S2p of mild steel obtained after immersion in CO_2-saturated solution at 2×10^{-4} mol·L^{-1} OIM-ME combination with a 4 hours immersion time at 65℃ (after fitting by origin 8.1).

The wide-scan XPS spectrum in Fig. 11 provides the evidence of the presence of S, C, N, O and Fe elements. The detected contents of C, S and N can be attributed to the presence of organic adsorption film formed on the carbon steel.

Fig. 12 presents the high-resolution spectrum of N1s of the film formed on carbon steel. The N1s peaks were targeted at 399.5 eV for each mixture. Their binding energy value is the same as that of N1s from the >C=N- bond in the OIM molecular [22]. Furthermore, it is observed that the area of N1s spectrum, which is associated with element content, is proportional to the addition amount of OIM. Fig. 13 presents the high-resolution spectrum of S2p, of which peaks are located at 162 eV for each mixture. It indicates the presence of thiol compounds which are usually detected with a binding energy of 162eV [34]. It reveals the existence of ME in the protective film.

In Fig. 14, two Fe2p3/2 peaks for each system of OIM-ME mixtures were obtained by fitting the XPS spectra with XPS peak 41 software. It is observed that here Fe element appears in two chemical states. The first one is $FeCO_3$ with a binding energy of 710.2 eV. And the second one is FeOOH with a binding energy of 712 eV. It is also observed that with the increase of ME in OIM-ME mixtures, the peak areas of $FeCO_3$ and FeOOH are decreasing. The presence of $FeCO_3$ should be the corrosion product of carbon steel exposed to CO_2-saturated NaCl solution [11]. In addition, the exposure of corrosion products ($FeCO_3$) to air could inevitably cause the hydrolysis and oxidation of $FeCO_3$ transforming into FeO/FeOOH [2].

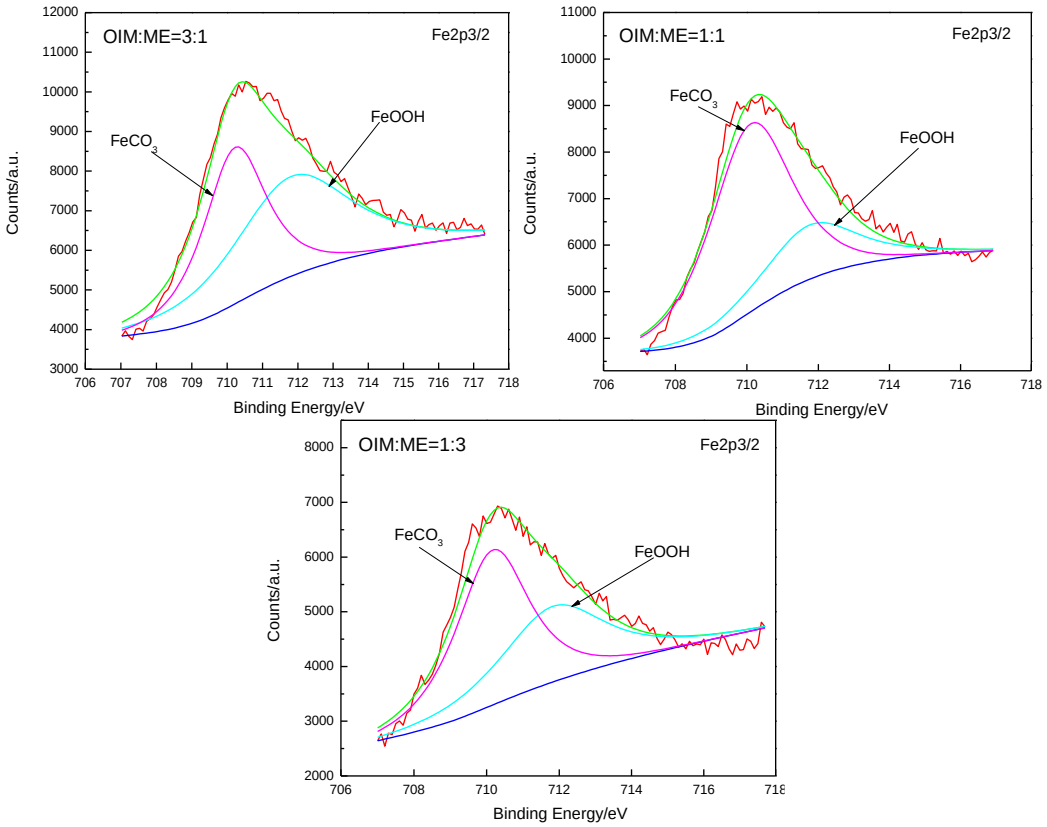

Figure 14. High-resolution XPS spectra of Fe2p3/2 of mild steel obtained after immersion in CO_2-saturated solution at 2×10^{-4} mol·L^{-1} OIM-ME combination with a 4 hours immersion time at 65°C.

Fig. 14 presents the result of deconvolution of O1s spectra. Here four chemical stats of oxygen have been observed. They are FeO*OH (the oxygen with *) with a binding energy of 530.1 eV, FeOO*H (the oxygen with *) with a binding energy of 531.2 eV, $FeCO_3$ with a binding energy of 531.9 eV and $HSCH_2CH_2OH$ (ME) with a binding energy of 529.6 eV [34], respectively. And a comparison of the peak areas of ME and $FeCO_3$ in each ratio of OIM-ME mixture suggests that there is a decrease in the amount of main corrosion products ($FeCO_3$) with the increase of ME in OIM-ME mixtures.

From above observation, it can be concluded that both OIM and ME are playing important roles in forming protective film on carbon steel in CO_2-saturated 3.5% NaCl solution.

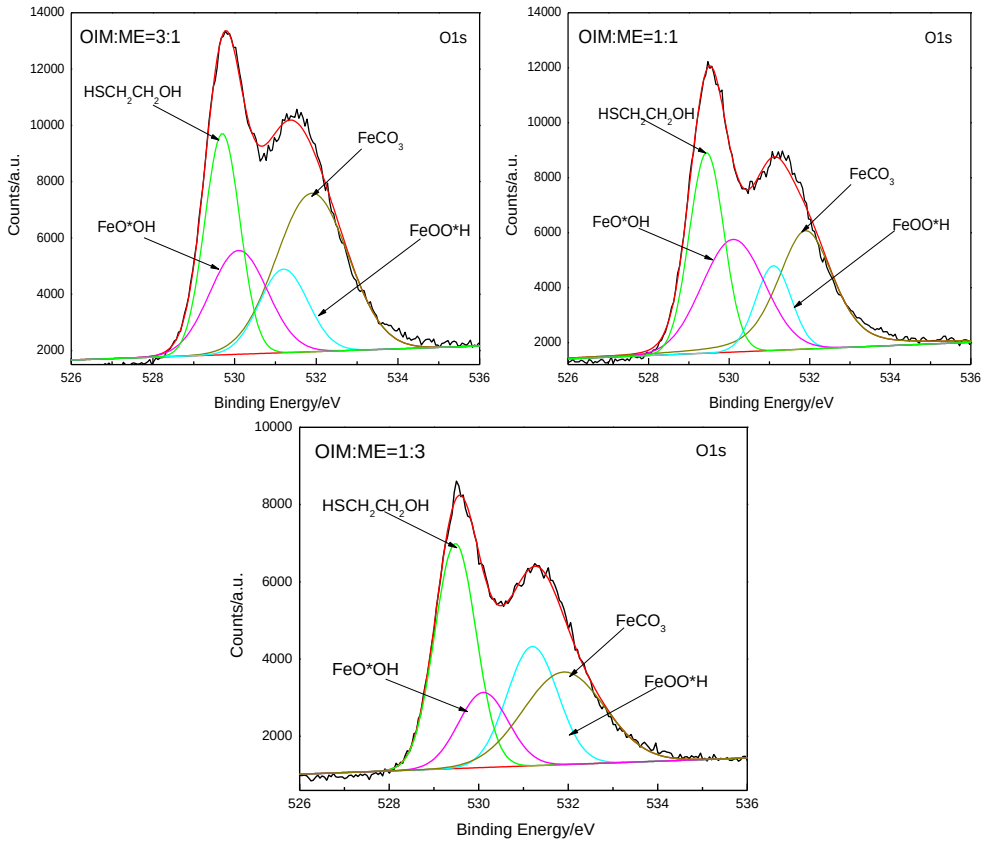

Figure 15. High-resolution XPS spectra of O1s of mild steel obtained after immersion in CO_2-saturated solution at 2×10^{-4} mol·L^{-1} OIM-ME combination with a 4 hours immersion time at 65°C.

3.5. Synergistic inhibition mechanism of OIM and ME

It has long been a difficult problem to give a convincing explanation of the adsorption mechanism of corrosion inhibitors in such corrosive medium containing complex ions, especially for synergistic inhibitors. Hard efforts were made in this paper to provide a proper adsorption model to elucidate the synergistic inhibition effect between OIM and ME. As mentioned above, two kinds of adsorption model are possible. They are alternative adsorption and bilayer adsorption models. But according to our experimental results, the bilayer adsorption model is preferred. As shown in Fig. 16, a bilayer adsorption film model is proposed to illustrate the synergistic inhibition mechanism between OIM and ME. In the

adsorption model, ME molecules form the inner layer and OIM molecules the role of the outer film barrier to block the corrosive media.

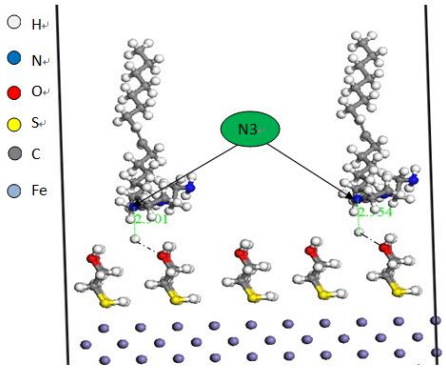

Figure 16. Bilayer film model for the synergistic corrosion inhibition effect of the OIM-ME combination in CO_2-saturated solution at 65°C.

Thiol compounds are capable of chemically binding to metals like Au, Fe etc. by sharing of electrons between S and metal atoms. Moreover, thiol compound like ME tends to self-assemble onto the metal surface to form highly ordered and compact films to protect the substrate from corrosion [35-37]. In terms of these facts, it is deduced that ME molecules with smaller volumes and greater polarity theoretically are more likely to adsorb with priority onto the surface of carbon steel, form chemical coordinate bond between -SH and Fe atom and self-assemble on carbon steel surface to behave as the inner protect layer.

As for the interaction between ME and OIM, Module b3lyp/6-31+g** in Gaussian 09 software was adopted to estimate it. Results suggest that, in vacuum, OIM could link to ME by hydrogen bond between N^3 in the imidazole ring of OIM and H atom in the hydroxyl group of ME. The hydrogen bond length is approximately 2.05 Å and the bond energy is about 43.56 $kJ \cdot mol^{-1}$. In real circumstances, such as CO_2-saturated 3.5% NaCl solution in this paper, the situation may be much more complicated and the interaction between molecules is quite difficult to be calculated by computing.

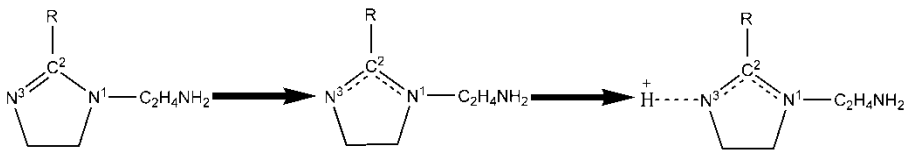

Figure 17. Graphical representation of protonation of OIM in CO_2-saturated solution [22]

However, theoretically there may be two forms of hydrogen bond between OIM and ME. The first possibility is that the hydrogen bond forms between N^3 in the imidazole ring of OIM and H atom in the hydroxyl group of ME, as described in the theoretical calculation in vacuum. As shown in Fig. 17,

the second possibility is that the N^3 atom in the imidazole ring of OIM preferentially protonated with H^+ in acidic solution [22]. And the ammonium ions of the protonated OIM bond to O atom in the hydroxyl group of ME. These two possibilities can coexist under certain circumstance. And it is proposed that the second situation is much more possible due to presence of a great quantity of H^+ in the solution.

This bilayer film model also can be supported by the evidence from EIS tests and equivalent circuit simulation as discussed in section 3.3. Firstly, the R_{ct} value of the outer interface, at the level of 10^4, is much larger than that of the inner interface which is at the level of 10^2 (Fig. 8). Secondly, when ME and OIM are independently used, the impedance modulus value of ME is smaller than that of OIM during all immersion time (Fig. 9) also can indicate the preferential adsorption of ME molecules onto carbon steel results in the lower R_{ct} of inner interface.

In conclusion, ME molecules adsorb onto carbon steel surface with priority by forming highly ordered and compact self-assembling films in the test solution. Then the protonated OIM molecules combine with ME molecules by hydrogen bond. Thus, a bilayer protective film is formed.

4. CONCLUSIONS

In this paper, the synergistic inhibition effect between OIM and ME was investigated by weight-loss method, electrochemical measurements and XPS surface analysis. The conclusions are summarized as follows:

(1) The synergistic inhibition effect was found between OIM and ME on the corrosion of carbon steel in 3.5% NaCl solution saturated with CO_2 at 65℃.

(2) The mixture exhibits the best synergistic corrosion inhibition effect when the molar ratio of OIM: ME equals to 1:3.

(3) OIM-ME mixture is a mixed-type corrosion inhibitor. And its corrosion inhibition efficiency can reach as much as 90% with 2×10^{-4} mol·L^{-1}.

(4) A bilayer adsorption model is proposed to illustrate the synergistic effect between OIM and ME. ME molecules adsorb onto carbon steel surface with priority by forming highly ordered and compact self-assembling films in the test solution. Then the protonated OIM molecules combine with ME molecules by hydrogen bond.

ACKNOWLEDGMENTS
This work was supported by the Department of Science and Technology of Sichuan Province (2020YJ 0363).

References

1. P. C. Okafor, Y. G. Zheng, *Corros. Sci.*, 51 (2009) 850-859.
2. T. Z. Zhu, L. D. Wang, W. Sun, M. Wang, J. S. Tian, Z. Q. Yanga, S. L. Wang, L. Xia, S. H. He, Y. Z. Zhou, G. C. Liu, *Corros. Sci.*, 140 (2018) 182-195.
3. R. Barker, D. Burkle, T. Charpentier, H. Thompson, A. Neville, *Corros. Sci.*, 142 (2018) 312-341.
4. W. H. Durnie, B. J. Kinsella, R. De Marco, A. Jefferson, *J. Appl. Electrochem.*, 31 (2001) 1221-1226.
5. E. Basilico, S. Marcelin, R. Mingant, J. Kittel, M. Fregonese, F. Ropital, *Mater. Corros.*, (2021) 1.
6. D. A. López, S. N. Simison, S. R. de Sánchez, *Electrochim. Acta*, 48 (2003) 845-854.

7. X. Liu, P. C. Okafor, Y. G. Zheng, *Corros. Sci.*, 51 (2009) 744-752.
8. D. M. Ortega-Toledo, J. G. Gonzalez-Rodriguez, M. Casales, L. Martinez, A. Martinez-Villafañe, *Corros. Sci.*, 53 (2011) 3780-3787.
9. X. D. Ren, H. Wang, Q. Wei, Y. Lu, B. W. Xiao, J. Xie, *Corros. Sci.*, 189 (2021) 109619.
10. T. Hong, Y. H. Sun, W. P. Jepson, *Corros. Sci.*, 44 (2002) 101-102.
11. J. K. Heuer, J. F. Stubbins, *Corros. Sci.*, 41 (1999) 1231-1243.
12. C.-O. A Olsson, D. Landolt, *Electrochim. Acta*, 48 (2003) 1093-1104.
13. D. A. López, W. H. Schreiner, S. R. de Sánchez, S. N Simison, *Appl. Surf. Sci.*, 207 (2003) 69-85.
14. M. Heydari, M. Javidi, *Corros. Sci.*, 61 (2012) 148-155.
15. M. A. Quraishi, M. Z. A. Rafiquee, S. Khan, N. Saxena, *J. Appl. Electrochem.*, 37 (2007) 1153-1162.
16. J. Tang, H. Wang, X. Q. Jiang, Z. H. Zhu, J. Xie, J. L. Tang, Y. Y. Wang, M. Chamas, Y. Q. Zhu, H. G. Tian, *Int. J. Electrochem. Sci.*, 13 (2018) 3625-3642.
17. X. Liu, Y. G. Zheng, *Corros. Eng. Sci.*, *Technol.*, 43 (2008) 87-92.
18. H. Wang, J. Tang, J. Xie, *Int. J. Electrochem. Sci.,* 12 (2017) 11017-11029.
19. C. Zhang, H. B. Duan, J. M. Zhao, *Corros. Sci.*, 112 (2016) 160-169.
20. D. X. Wang, S. Y. Li, Y. Ying, M. J. Wang, H. M. Xiao, Z. X. Chen, *Corros. Sci.*, 41 (1999) 1911-1919.
21. J. Zhang, X. L. Gong, H. H. Yu, M. Du, *Corros. Sci.*, 53 (2011) 3324-3330.
22. J. M. Zhao, G. H. Chen, *Electrochim. Acta*, 69 (2012) 247-255.
23. P. C. Okafor, C. B. Liu, X. Liu, Y. G. Zheng, *J. Appl. Electrochem.*, 39 (2009) 2535-2543.
24. J. Z. Ai, X. P. Guo, J.E. Qu, Z. Y. Chen, J.S. Zheng, *Colloids Surfaces A Physicochem. Eng. Asp*., 281 (2006) 147-155.
25. P. C. Okafor, C. B. Liu, X. Liu, Y. G. Zheng, F. Wang, C. Y. Liu, *J. Solid State Electrochem.*, 14 (2009) 1367-1376.
26. C. D. Wagner, W. N. Riggs, L. E. Davies, J. F. Moulder, G. E. M. (Eds.), *Physical E, Perkin-Elmer Corp.*, 1979.
27. B. M. Mistry, S. K. Sahoo, S. Jauhari, *J. Electroanal. Chem.*, 704 (2013) 118-129.
28. C. Cao, *Corros. Sci.*, 38 (1996) 2073-2082.
29. K. F. Khaled, N. Hackerman, *Electrochim. Acta*, 48 (2003) 2715-2723.
30. B. S. Hou, Q.H. Zhang, Y. Y. Li, G.Y. Zhu, G. A. Zhang, *Corros. Sci.*, 166 (2020) 108442.
31. G. A. Zhang, C. F. Chen, M. X Lu, C. W. Chai, Y. S. Wu, *Mater. Chem. Phys.*, 105 (2007) 331-340.
32. M. P. Desimone, G. Grundmeier, G. Gordillo, S. N. Simison, *Electrochim. Acta*, 56 (2011) 2990-2998.
33. V. M. Huang, S. L. Wu, M. E. Orazem, N. Pébère, B. Tribollet, *Electrochim. Acta,* 56 (2011) 8084
34. K. Nozawa, H. Nishihara, K. Aramaki, *Corros. Sci.*, 39 (1997) 1625-1639.
35. F. Pak, K. Meral, R. Altundaş, D. Ekinci, *J. Electroanal. Chem.*, 654 (2011) 20-28.
36. G. J. Lim, H. J. Hwang, J. H. Kim, *Anal. Biochem.*, 419 (2011) 205-210.
37. V. Ganesh, S. K. Pal, S. Kumar, V. Lakshminarayanan, *Electrochim. Acta*, 52 (2007) 2987-2997
38. 38. F.G. Liu, M. Du, J. Zhang, M. Qiu, *Corros. Sci.*, 51 (2008) 102-109.
39. B. Wang, M. Du, J. Zhang, *Adv. Mater. Res.*, 865 (2009) 981-984.
40. J. Zhang, L. W. Niu, F. M. Zhu, C. J. Li, M. Du, *J. Surfactants Deterg.*, 16 (2013) 947-956.